

Strong Catalyst–Support Interactions in Electrochemical Oxygen Evolution on Ni–Fe Layered Double Hydroxide

Haoyang Gu, Guoshuai Shi, Hsiao-Chien Chen, Songhai Xie, Yingzhou Li, Haonan Tong, Chunlei Yang, Chenyuan Zhu, J. Tyler Mefford, Heyi Xia, William C. Chueh, Hao Ming Chen, and Liming Zhang*

Cite This: *ACS Energy Lett.* 2020, 5, 3185–3194

Read Online

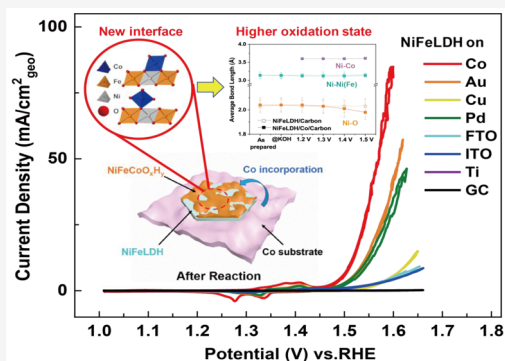
ACCESS |

Metrics & More

Article Recommendations

Supporting Information

ABSTRACT: Strong catalyst–support interaction plays a key role in heterogeneous catalysis, as has been well-documented in high-temperature gas-phase chemistry, such as the water gas shift reaction. Insight into how catalyst–support interactions can be exploited to optimize the catalytic activity in aqueous electrochemistry, however, is still lacking. In this work, we show the rationally designed electrocatalyst/support interface can greatly impact the overall electrocatalytic activity of Ni–Fe layered double hydroxide (NiFeLDH) in water oxidation. In particular, the use of Co as a non-noble metal support greatly improves the activity of NiFeLDH 10-fold compared to the traditional electrocatalytic supports such as fluorine-/indium-doped tin oxide (FTO/ITO) and glassy carbon. We attribute the activity enhancement of NiFeLDH/Co to the *in situ* formation of a porous NiFeCoO_xH_y layer via Co incorporation, which dramatically promotes the redox chemistry of metal centers on the outer surface and enhances the electrical conductivity of the catalyst over 2 orders of magnitude. This new discovery highlights the importance of a rationally designed electrocatalyst/support interface and offers a new paradigm for designing and developing highly active electrocatalytic systems via marrying catalyst and support and creating synergy.



Strong catalyst–support interaction crucially affects overall catalytic performance, as has been well-established in the high-temperature water gas shift reaction since the 1970s.¹ This phenomenon, derived from either bonding interactions^{2–4} or electronic perturbations,⁵ was first demonstrated on the interface of group VIII metal clusters (as catalysts) and reducible transition-metal oxides (as supports) and recently has been extended to noble metals on other supports, such as phosphates,⁶ carbides,^{7–10} and hydroxides.¹¹ The strong interaction between catalyst and support, generally introduced by the high-temperature H₂ or O₂ treatment in the gas phase, decreases the activation barrier for water dissociation, and stabilizes the absorbed intermediates on the active sites. One interesting related question is whether such strong catalyst–support interaction exists on the solid–liquid interface in aqueous electrocatalysis at ambient temperature. In the previous studies, people pursued inert conductive supports as current collectors, and developed numerous strategies to optimize the catalytic efficiency by engineering the chemical composition and/or morphological geometry of the electrocatalysts, i.e., to improve the turnover rate of reaction at the interface of catalyst/electrolyte.^{12,13}

However, much less attention has been focused on the catalyst/support interface, which also demonstrates the ability to affect the overall catalytic activity, as confirmed by recent studies on the semiconductive catalyst/metallic current collector interface with a Mott–Schottky junction.^{14,15} Although this synergistic effect between catalyst and support is essential, few works to date emphasized the contributions from supports, in particular the kinetically unstable supports, in aqueous electrocatalysis.

Potential application of fuel generation with renewable electricity requires efficient, cost-effective, and durable electrocatalysts.¹⁶ The bottleneck in developing water-splitting technology is the kinetically slow water oxidation, the oxygen-evolution reaction (OER), which involves the transfer

Received: July 23, 2020

Accepted: September 15, 2020

Published: September 15, 2020

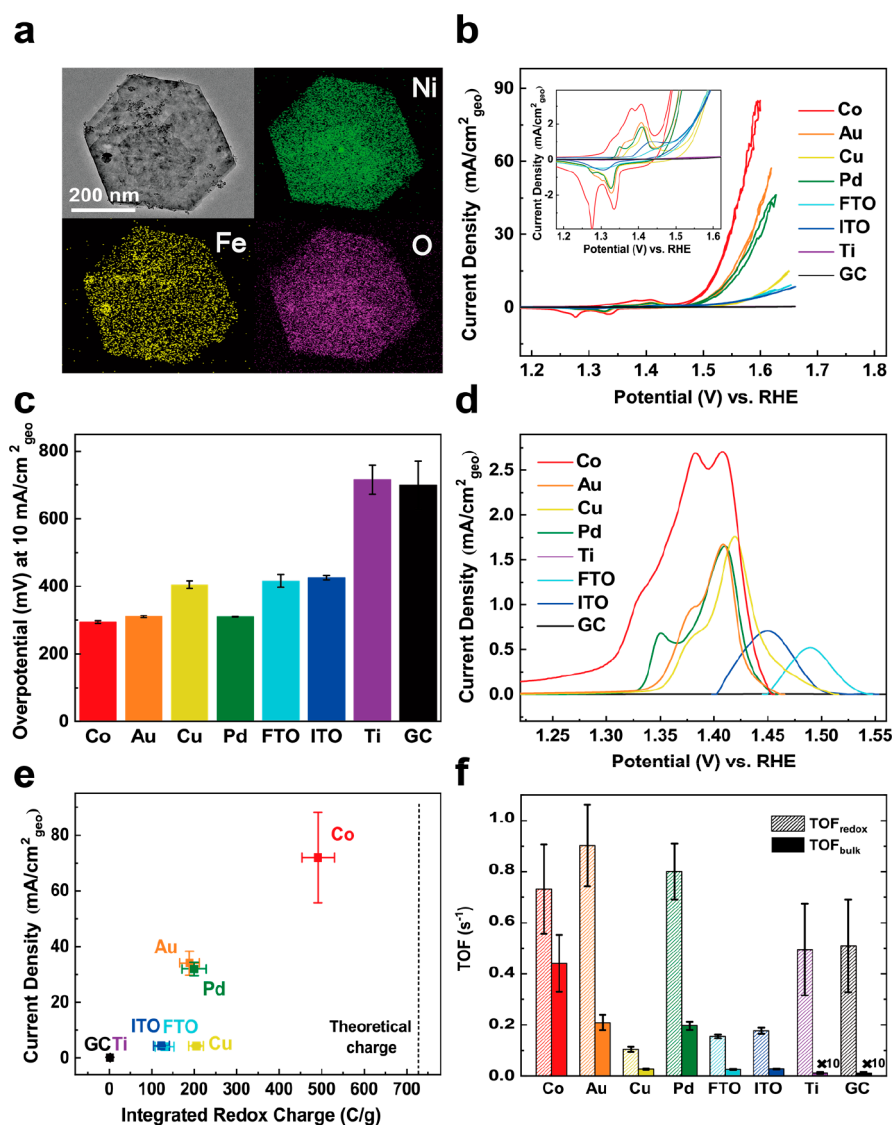


Figure 1. Distinguished OER activities of NiFeLDH on various supports. (a) TEM and EDX elemental mapping of one NiFeLDH hexagonal flake. (b) CV of NiFeLDH on various supports. Inset shows enlarged view of the distinguished precatalytic redox features (sweeping rate, 10 mV/s). (c) Comparison of the overpotentials at 10 mA/cm²_{geo} on different supports. (d) Comparison of the oxidation redox peaks of NiFeLDH on various supports (sweeping rate, 10 mV/s) after subtracting OER current using Butler–Volmer equation. (e) Correlation between the geometric current density of NiFeLDH at $\eta = 350$ mV and the integrated charge from the oxidation peaks shown in panel d on different supports. The dashed line indicates the theoretical integrated redox charge for a complete conversion, assuming all deposited Ni was oxidized to Ni³⁺. (f) TOF calculated from the total mass (TOF_{bulk}) and the Ni redox peak (TOF_{redox}, e⁻ per Ni) of NiFeLDH at $\eta = 350$ mV on various supports. The TOF_{bulk} of Ti and GC were magnified 10 times for clarity. All the activity measurements were performed with an identical geometric catalyst loading in an O₂-saturated 1 M KOH electrolyte (pH 13.8), and the error bars represent the standard deviation of triplicate measurements.

of four electrons and four protons.¹⁷ As one of the most efficient earth-abundant electrocatalysts for OER in alkaline electrolytes, nickel–iron layered double hydroxide (NiFeLDH) has been studied for over 30 years;^{18,19} however, the science is still under intense debate,^{20–30} mostly because the dynamic restructuring and phase transformation of this type of catalyst make understanding the electrocatalytic response, in terms of fundamental processes, difficult. For instance, the role of Fe is still elusive.^{21,22,24,25,27,30,31} Pure Ni(OH)₂ is a poor OER catalyst, but the activity drastically increases when Fe is incorporated, with the optimal activity for compositions between 10% and 50%.^{21,22,26,32} To date, the activity optimization of transition-metal-based oxides/hydroxides predominantly focuses on engineering the composition

and/or geometry of the catalysts to improve the turnover rate.^{29,33–35} Much less is known about how catalyst–support interactions could affect the overall activity of this heterogeneous catalyst. Previous studies have demonstrated that carbon-based materials like carbon nanotubes²⁰ and graphite foams³⁶ are capable of improving the catalytic efficiency of hydroxides as conductive supports because of their high electron conductivity as well as large surface area. Oxide and sulfide nanoarrays^{37–39} could also serve as supports for Ni- and Fe-based hydroxides, with lattice strain introduced on the catalyst–support interface and thereby enhancing the catalytic performance. Recently, some studies indicate that OER activities of Ni and Co oxides could be promoted by noble metal substrates, such as Au,^{6,40–45} possibly because of the

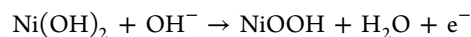
electronic interactions between catalyst and support. However, the detailed interfacial atomic structure and mechanisms of such enhancement are not entirely clear. It is evident that more efforts should be undertaken to assess whether and how the strong catalyst–support interaction affects the apparent electrocatalytic activity at ambient temperature in aqueous electrocatalysis.

Here, we demonstrate a strong interaction at the interface between NiFeLDH and support for water oxidation. Eight types of “flat” conductive supports are explored in this work, including metal foils (such as Au, Pd, Co, Cu, and Ti), conductive metal oxides (such as ITO and FTO), and glassy carbon (denoted as GC). A remarkable finding is that under equivalent electrochemical conditions, the OER activity of NiFeLDH on different supports are notably distinguished, having a linear-correlation with the *in situ* generation efficiency of oxidative Ni sites from the redox chemistry, which happens before OER. In particular, Co support dramatically boosts the activity of NiFeLDH 10-fold in comparison with FTO, ITO, and GC, all of which are widely used conductive substrates for electrocatalysis. The electronic coupling between NiFeLDH and support was also assessed by exploring the kinetics of interfacial charge transfer using a $[\text{Fe}(\text{CN})_6]^{3+/4+}$ redox probe. Atomic force microscopy (AFM), transmission electron microscopy (TEM), X-ray photoelectron spectroscopy (XPS), *in situ* X-ray absorption spectroscopy (XAS), and *operando* catalyst conductivity measurements were carried out to reveal that the activity of NiFeLDH/Co is largely improved by the *in situ* incorporation of Co into NiFeLDH during OER. The formation of porous NiFeCoO_xH_y dramatically increases the production of activated Ni sites on the outer surface, as confirmed by the kinetics study on the precatalytic redox response, and increases the conductivity of the catalyst over 2 orders of magnitude. Taking advantage of the strong catalyst–support interaction, we fabricated NiFeLDH on a high-surface-area Co foam and achieved 300 mA/cm² current density at 310 mV overpotential, alongside ~95% Faradaic efficiency and good stability over 90 h. Our work illuminates the importance of well-designed catalyst–support interface for electrocatalysis and represents an attractive alternative to the established catalyst engineering strategies for enhancing the aqueous electrocatalytic activity.

Distinguished OER Activities on Different Supports. NiFeLDH was synthesized via a modified hydrothermal procedure (see Experimental Methods in the Supporting Information for details).⁴⁶ The morphology of as-grown NiFeLDH consists of well-crystallized hexagonal flakes with a lateral dimension of 300–500 nm and a thickness of tens of nanometers (Supplementary Figures 1–3). According to the energy dispersive X-ray analysis (EDX), Ni and Fe distribute uniformly across the flake (Figure 1a). To achieve a better catalytic efficiency, we optimized the composition stoichiometry (Supplementary Figure 4) and observed that the nominal 25 mol % Fe doped NiFeLDH (Ni:Fe = 3:1) shows the best OER catalytic activity, which is consistent with previous reports.²¹ NiFeLDH was then dispersed uniformly in ethanol, drop-cast onto various flat conductive supports with an equivalent loading amount to form a uniform electrocatalyst film. The average molar loading amounts of Ni and Fe on various substrates are $0.439 \pm 0.009 \mu\text{mol}/\text{cm}^2$ and $0.114 \pm 0.003 \mu\text{mol}/\text{cm}^2$, respectively, measured by inductively coupled plasma optical emission spectrometry (ICP-OES). The root-mean-square average of height deviation of the bare

supports was first measured to exclude the possible geometric effects (Supplementary Figure 5). Figure 1b compares the stable cyclic voltammetry (CV) of NiFeLDH on different supports in a 1 M KOH solution (pH 13.8), which unambiguously demonstrates different OER activities and precatalytic redox features. More rigorous data sets showing the activity trend of the NiFeLDH on different supports are provided in Supplementary Figures 6 and 7. In particular, NiFeLDH supported on Co foil shows a dramatically higher OER current in comparison with those on other substrates; for example, at an overpotential of 300 mV, the current of NiFeLDH/Co achieves 20 mA/cm², ~2× more active than the catalyst loading on Au, which was regarded as the most efficient conductive support because of a high electro-negativity.^{6,40} Moreover, the OER current density of NiFeLDH/Co is confirmed to outperform that of NiFeLDH/Au at various catalyst loading conditions (Supplementary Figure 8), excluding the possible thickness-dependent effect of the catalyst.²¹ Surprisingly, FTO, ITO, and GC, the commonly used current collectors for electrocatalysis, are not good supports for the hydrothermally synthesized NiFeLDH crystal. The OER activities of pure conductive supports were also tested for comparison (Supplementary Figure 9), to exclude the catalytic contributions from bare substrates at the interested potential region. Figure 1c and Supplementary Figure 10 summarize the overpotentials required to drive a geometric current density of 10 mA/cm² and 100 mA/cm² on different supports, respectively. The current comparison with a long durable time was performed to exclude the possibility of deactivation from the peeling off of NiFeLDH catalyst (Supplementary Figure 11).

Another important distinguishing feature between the cyclic voltammetry curves on different supports lies in the precatalytic redox features. The redox wave corresponds to, nominally, evolution of the oxidation state of the metal cation, and the size of the redox wave can serve as a valuable feature to evaluate the number of metal atoms participating in the reaction.⁴⁷ Because Fe generally exhibits no redox feature (Supplementary Figure 12), we assume the electrochemical activation mainly occurs on Ni atoms, with a redox reaction of



One electron transfer was assumed in the redox; however, we caution that the active material may involve Ni in nominal oxidation states higher than 3⁺. The Ni redox peaks on various supports are observed inconsistently, likely because of the oxidation/reduction of Ni having different local coordination structures with Fe and support metal ions. In comparison with FTO and ITO, Co support obviously reduced the Ni redox potential. However, no obvious shift of Ni redox peak was observed on Co compared with those using Au and Pd as conductive supports. To perform an accurate redox peak integration, background OER current was subtracted using an exponential function based on the Butler–Volmer equation (Figure 1d and Supplementary Figure 13, see Experimental Methods in the Supporting Information). The formation of Ni sites with higher oxidation states is essential to the following OER process, and indeed, we observed a “rough” linear correlation between the integral of redox wave and the OER activity on different substrates (Figure 1e, the geometric OER current density is picked up at $\eta = 350$ mV), indicating the OER activity of NiFeLDH strongly depends on the *in situ*

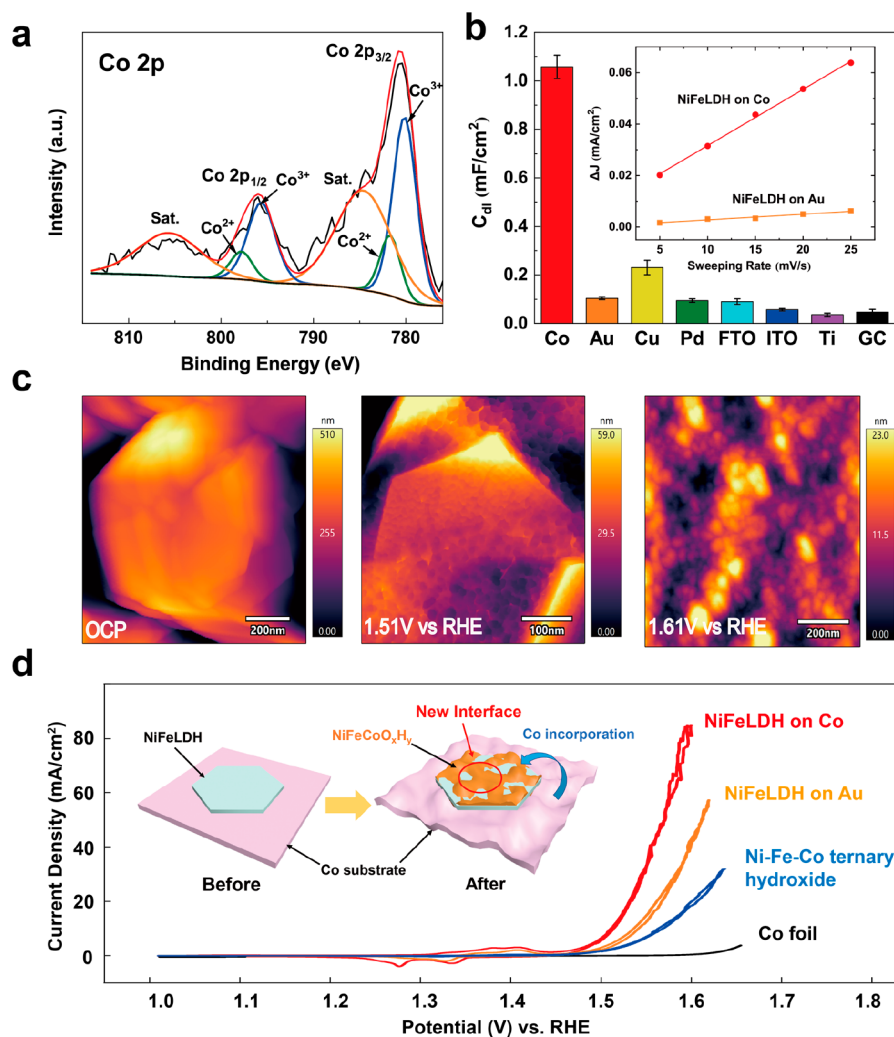


Figure 2. Physical characterization of NiFeLDH/Co after OER. (a) XPS Co 2p spectra of NiFeLDH after electrocatalysis, showing the mixed valence states of Co²⁺ and Co³⁺. (b) Comparison of the C_{dl} of NiFeLDH loaded on different conductive supports after electrochemical measurements in a 1 M KOH electrolyte. Inset shows the linear behavior of ΔJ (defined as the difference between anodic and cathodic currents) as a function of sweeping rate for NiFeLDH loaded on Au and Co supports. (c) AFM figures of NiFeLDHs on a Co-coated silicon chip at open-circuit potential, 1.51 V vs RHE and 1.61 V vs RHE. (d) CVs of NiFeLDH on Co, NiFeLDH on Au, Ni–Fe–Co ternary hydroxides and bare Co foil in 1 M KOH at a sweeping rate of 10 mV/s, showing the interface between NiFeLDH and Co foil is crucial to enhance OER. Inset shows the schematic illustration highlighting the importance of the catalyst/support interface.

generation efficiency of metal active sites, which happens before and in-tandem with OER.

To show the intrinsic activity on different supports, we converted the activity into the turnover frequency (TOF), the number of O₂ molecules generated per active site per unit time, using two estimates for the number of active sites and assuming a unity Faradaic efficiency for O₂ generation. TOF_{bulk} assumes all the deposited metal atoms (Ni + Fe) are active, and TOF_{redox} assumes one active site per transferred electron in the redox wave. As shown in Figure 1f, the TOFs thus calculated show different trends on various supports (see Experimental Methods in the Supporting Information). Co exhibits the best TOF_{bulk} ~0.4 ± 0.1 s⁻¹ at η = 350 mV. However, Au shows the highest TOF_{redox} ~0.9 ± 0.2 s⁻¹ at η = 350 mV, consistent with previous reports that the high electronegativity of Au assists to stabilize oxidative Ni sites, making those “hot spots” more efficient when performing water oxidation.^{6,40–45,48} In contrast, Co is not an excellent metal support in terms of TOF_{redox}. However, Co boosts the

population of metal active sites, ~2.5X in comparison with Au, leading to an excellent apparent OER catalytic activity.

Physical Characterization of NiFeLDH/Co after OER. We next rationalize why the generation of metal active sites is much enhanced on Co. Such unexpected distinction is likely to be caused by the different charge injection barriers across catalyst/support interfaces. We first assess the interfacial electron transport using a fast-redox couple [Fe(CN)₆]^{3+/4+}, which has a similar and well-defined redox position as OER (OH⁻/O₂) in 1 M KOH.^{49,50} Indeed, the cyclic voltammograms show different behaviors on various substrates (Supplementary Figure 14). Significant rectification is shown on Ti, FTO, ITO, and GC, which corresponds to a large Schottky barrier on the interface and can well explain the weak electrochemical response toward OER (Supplementary Figure 15). All the other substrates, such as Au, Co, Pd, and Cu foils, exhibit a symmetric redox peak with a sweeping rate-independent anodic/cathodic peak shift of 60–70 mV (Supplementary Figure 16), suggesting the absence of an electron injection barrier. We further correlated the anodic/cathodic peak shift

with the charge-transfer resistance measured from the electrochemical impedance spectroscopy and observed a strong positive correlation (Supplementary Figure 17). Our observation demonstrates that the interface between catalyst and support plays an important role in determining the overall electrocatalytic activity. However, these results are insufficient to explain the dramatic current enhancement on Co in comparison with Au, Pd, and Cu, on which the charge transfer across the interface is not a limitation, suggesting that there must be some other synergetic effects between the catalyst and the support.

To determine whether the morphology and/or surface composition of electrode change during OER, representative NiFeLDH/Co samples were characterized after electrocatalysis. TEM and EDX analysis demonstrate an obvious Co signal was observed across the flakes (Supplementary Figure 18 and Table 1), indicating Co was introduced into NiFeLDH under a positive bias. To compare, we tested the elemental distribution of NiFeLDH loaded on Au after OER, and no obvious Au signal was observed (Supplementary Figure 19 and Table 2). The appearance of Co on NiFeLDH is also confirmed by the *ex situ* XPS measurement, which shows that $\sim 2\%$ Co arises after OER, with mixed valence states of 2^+ and 3^+ (Figure 2a). The amount of Co also excludes the significant charge contribution of Co to the redox charge.

To further investigate the change in surface area, the double-layer capacitance (C_{dl}) was measured after OER (Figure 2b). Surprisingly, the C_{dl} of NiFeLDH/Co increases over 10-fold compared to NiFeLDH on other supports, suggesting a strong improvement of the electrochemical accessibility. We also notice that the C_{dl} of NiFeLDH/Cu slightly increases after OER; however, this structure transformation has no effect on improving the subsequent OER performance. Furthermore, the *ex situ* AFM tests were performed to monitor the morphological change of NiFeLDH nanosheets (Figure 2c). With the applied bias increasing from OCP to 1.61 V vs RHE, the hexagonal flakes of NiFeLDH gradually collapse, especially on the edges and corners. The transition of a single nanosheet into disordered nanoparticles can be clearly observed, as previously reported by Boettcher et al.⁵¹ At the same time, we observed the roughening of Co and the emerging of an amorphous layer on NiFeLDH. This is direct evidence of the moving process of Co from substrate to NiFeLDH, and such a process also explains the 10 \times increase of C_{dl} after reaction. On the other hand, NiFeLDH flakes drop-cast on highly ordered pyrolytic graphite (HOPG) remain rather intact even at the potential of 1.61 V vs RHE (Supplementary Figure 20), with no obvious cracks or increased roughness observed. The direct comparison confirms that the existence of Co support facilitates the reconstruction of NiFeLDH as mentioned before.

We also observed that the interface between NiFeLDH and Co foil is critical for the OER activation. As shown in Figure 2d, the comparison of OER electrocatalysis between NiFeLDH/Co and bare Co foil evidenced that the generation of pure CoO_xH_y cannot dramatically boost the OER activity, which indicates the incorporation of Co into NiFeLDH to generate $\text{NiFeCoO}_x\text{H}_y$, rather than the CoO_xH_y deposition, is crucial to the activity enhancement. The enhanced OER also cannot be observed when intentionally and uniformly introducing Co into the bulk structure of NiFeLDH, namely, employing the as-synthesized Co–Ni–Fe ternary hydroxides as an electrocatalyst (XRD, TEM, with EDX analysis and more

electrochemistry on ternary hydroxides with different stoichiometry of Co/Ni/Fe are shown in Supplementary Figures 21–25 and Supplementary Table 3). All of these results highlight the importance of the *in situ* formation of $\text{NiFeCoO}_x\text{H}_y$ through interfacial incorporation of Co under OER operating conditions (inset of Figure 2d), which is the key to promote OER.

In situ Electronic and Structural Characterization. The support-dependent local structure and chemical states of NiFeLDH/Co during OER were examined using *in situ* XAS, at the Ni and Fe K-edges. For data collection, a piece of Co-coated carbon paper (denoted as Co/carbon) instead of Co foil was used as the conductive support because of the strong background of Co signal from Co foil. NiFeLDH was drop-cast onto Co/carbon (denoted as NiFeLDH/Co/carbon) and assembled onto a special-designed cell, using Ag/AgCl and a carbon rod as the reference and counter electrode, respectively. The control experiment was conducted on NiFeLDH directly immobilized on a carbon paper (denoted as NiFeLDH/carbon). The Ni and Fe K-edges were recorded at the chronoamperometric condition with various given potentials. The energy positions of Ni K-edge gradually shifted toward a higher energy with the increase of the applied potential on both NiFeLDH/carbon and NiFeLDH/Co/carbon, indicating Ni^{2+} was oxidized to a higher chemical state under OER operating conditions (Figure 3a,b). Importantly, a large pronounced potential-induced edge-shift was in evidence on NiFeLDH/Co/carbon than that of NiFeLDH/carbon, i.e., the spectra showed a distinct edge-shift of ~ 0.6 eV at a potential of 1.5 V vs RHE and ~ 1.3 eV at 1.6 V vs RHE, whereas almost no obvious edge-shift was observed until 1.6 V vs RHE was applied without a Co interlayer. According to the edge shift, the averaged oxidation states of Ni were calculated to be 3.0 and 2.4 with and without Co support, respectively, at 1.6 V vs RHE.⁵² It is notable that there is a large discrepancy on Ni oxidation states under OER conditions in the reported literature,^{22,25} possibly because of the distinguished catalyst loading amount, pH of electrolyte, and applied potentials. However, the different edge shifts of NiFeLDH at equivalent conditions except for the applied supports strongly suggest that Co can promote the generation of Ni oxidative sites. In contrast to the unambiguous edge-shift of Ni K-edge, Fe K-edge demonstrates little shift throughout the reaction potential (Supplementary Figure 26), likely because of the trace amount of Fe^{4+} generation below the detection limit and/or the extremely short lifetime of produced Fe^{4+} . These spectroscopy results are consistent with the electrochemical redox behavior shown in CV, where Ni exhibits strong redox waves while Fe exhibits no features. The K-edge positions and average oxidation states for Ni and Fe at different potentials are summarized in Supplementary Tables 4 and 5.

The bond length of the first metal–oxygen shell is a characteristic of the oxidation states of metal ions. Here we performed the Fourier transform extended X-ray absorption fine structure (FT-EXAFS) analysis to investigate the local structural change of Ni and Fe during OER (see the fitting results in both *R* and *k* space, Figure 3c,d and Supplementary Figures 27–29). As shown in Figure 3c, the first peak at an apparent distance of ~ 1.5 Å and the second peak at ~ 2.7 Å are attributed to the single scattering path of the closest oxygen (e.g., Ni–O) and the second neighboring metal atoms (e.g., Ni–Ni(Fe)) surrounding the absorbing Ni atoms, respectively. The initial NiFeLDH exhibits a 6-fold coordination of Ni and

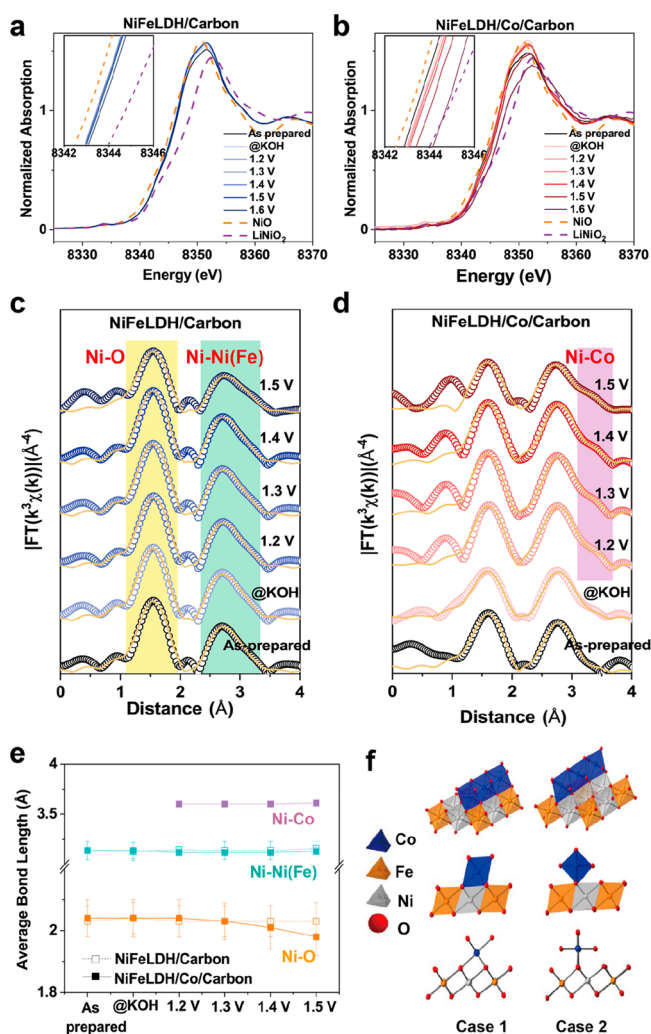


Figure 3. *In situ* Ni K-edge XAS spectra of NiFeLDH with and without Co support. (a and b) *In situ* Ni K-edge XANES spectra of (a) NiFeLDH/carbon and (b) NiFeLDH/Co/carbon. The spectra of NiO and LiNiO₂ were overlaid as references. Insets show the enlarged view of the potential-induced Ni K-edge shift. (c and d) R-space Ni K-edge EXAFS spectra of (c) NiFeLDH/carbon and (d) NiFeLDH/Co/carbon. Shown are experimental data and corresponding fitting curves (yellow line). (e) Average bond lengths extracted from EXAFS fitting, plotted as a function of applied potential. More fitting parameters are summarized in Supplementary Table 6. (f) Two proposed structural models of NiFeLDH/Co/carbon after electrocatalysis. The detailed local structures are depicted and discussed in the Supplementary Note 2 and Figure 35.

Fe, with an average Ni–O bond length of 2.04 Å and Fe–O bond length of 1.96 Å, respectively, indicating the predominate Ni²⁺ and Fe³⁺ nature (see the fitting results in Supplementary Tables 6–7). As shown in Figure 3e, with a Co layer underneath, the average Ni–O bond length decreased to 2.01 Å at 1.4 V vs RHE and further to 1.98 Å at 1.5 V vs RHE, confirming the generation of mixed states of Ni²⁺/Ni³⁺. At the same applied potential, the contraction of the Ni–O bond on NiFeLDH/carbon was barely observed, revealing that the generation of oxidative Ni sites is largely promoted by Co. Additionally, the average coordination number of the first Ni–O shell, as shown from the FT-EXAFS fitting, slightly decreased with the contraction of the Ni–O bond because

of the partial break of the lamellar structure (Supplementary Table 6).

Moreover, with a Co layer underneath, the average Fe–O bond length decreased to 1.91 Å at 1.5 V vs RHE, which is much shorter than that of NiFeLDH/carbon (1.97 Å). The average coordination number of the first Fe–O shell of NiFeLDH/Co/carbon is also less than that of NiFeLDH/carbon at the same potential (Supplementary Table 7). These results suggest that Co also promotes the generation of higher oxidative Fe sites, which are regarded as active sites of OER in a previous study.⁵³ It is also notable that the evolution of Fe–O bond length and coordination number with potential demonstrate a similar trend with Ni–O (Supplementary Figure 28 and Supplementary Table 7), likely because the coordination environment of Fe–O could be affected by the oxidation of Ni, which is also consistent with the previous work.⁵² More bond lengths of the Ni-, Fe-, and Co-based oxides/hydroxides before and after electrolysis from previous reports are shown in Supplementary Table 8.

A stronger distinction between NiFeLDH/Co/carbon and NiFeLDH/carbon was observed when taking the second shell metal–metal distances into account. As shown in Figure 3e, Co appears in the second shell of Ni coordination environment when the potential is higher than 1.2 V vs RHE, as evidenced from the side peak at ~3.3 Å in the FT-EXAFS results in Figure 3d (the overlaid curves are shown in Supplementary Figure 30). If performing EXAFS fitting without Ni–Co path, the fitting curve shows a large discrepancy with the experimental curve, especially at a higher radial distance, suggesting the formation of Ni–Co bonds at operating conditions (Supplementary Figure 31). These results are well consistent with the higher-energy shift of Co–K edge under a positive bias, indicating that the Co support was oxidized and incorporated into NiFeLDH at the basic condition (Supplementary Figure 32). The K-edge positions and average oxidation states for Co element are summarized in Supplementary Table 9. The K-edge of Co exhibited a shift of ~0.4 eV under a potential of 1.5 V vs RHE, indicating the oxidation of Ni. Additionally, the FT-EXAFS fitting of Co K-edges in both *R* and *k* space showed a formation of second neighboring metal atoms of Co–Ni bond with the bond length of 3.6 Å under a potential of 1.2 to 1.5 V vs RHE (Supplementary Figures 33–34 and Table 10). This phenomenon was in agreement with the results of FT-EXAFS fitting of Ni K-edges. We did not observe an obvious Fe–Co path when performing EXAFS fitting (Supplementary Figures 28 and 29), indicating that Co ions prefer to bond with Ni–O rather than Fe–O, which could be caused by the difference of Co adsorption energy between Ni–O and Fe–O.⁵⁴ It is notable that the average Ni–Co distance (~3.6 Å) is much larger than that of Ni–Ni(Fe) (~3.2 Å) in NiFeLDH, indicating that there is a Ni–Co path with a specific long distance in the *in situ* produced NiFeCoO_xH_y. We also observed that the coordination number of Ni–Co is remarkably smaller than that of Ni–Ni(Fe) (Supplementary Table 6), and we attributed this to the formation of small nanosize clusters where the Co ions at the edges have fewer Co–Ni interactions than those in the center, thus decreasing the overall mean Ni–Co coordination numbers. We also envision that the Co ions are not located in the bulk of NiFeLDH; otherwise the Ni–Co distance will be much shorter and the coordination number will be close to 6, as shown by

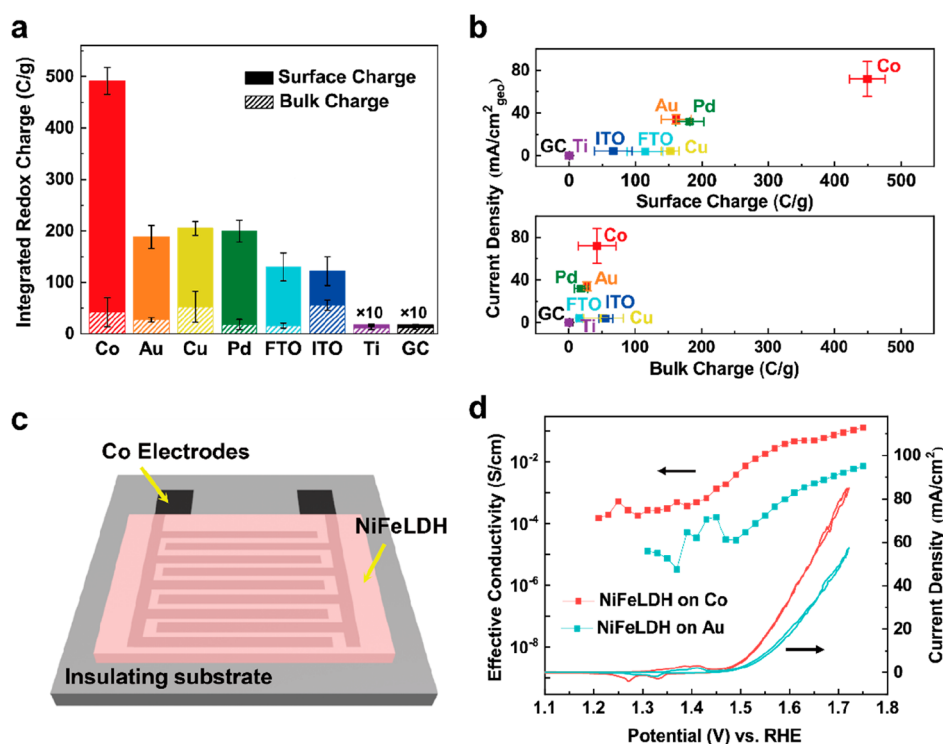


Figure 4. Improved $\text{Ni}^{2+}/\text{Ni}^{3+}$ redox chemistry and enhanced catalyst conductivity. (a) Redox charge integrated from the forward redox wave of NiFeLDH on various supports, showing the charge distribution in the bulk (hatched) and on the surface (solid) of catalyst, respectively. (b) Correlation between the current density of NiFeLDH at $\eta = 350$ mV and the integrated surface (top panel) and bulk (bottom panel) charge of the forward redox wave on different supports. All the measurements are performed in an O_2 -saturated 1 M KOH electrolyte (pH 13.8) with a sweeping rate of 10 mV/s, and the error bars represent the standard deviation of triplicate measurements. (c) Schematic illustration of the interdigital dual-working electrode with electrocatalyst coating. (d) Steady-state effective conductivity of NiFeLDH on an interdigitated array of Co (red) and Au (blue) electrode as a function of applied potential in an O_2 -saturated 1 M KOH. CV curves with a sweeping rate of 10 mV/s are overlaid.

the Ni–Ni(Fe) scattering path in NiFeLDH. Given the average Ni–Co distance is $\sim 2\times$ longer than that of Ni–O, we propose two structural models to demonstrate the possible locations of Co ions (Figure 3f), where each CoO_6 octahedron shares 3 (case 1) or 2 (case 2) bridging oxygen atoms with the underlying Ni(Fe) O_6 octahedron. The detailed proposed local structures of $\text{NiFeCoO}_x\text{H}_y$ are depicted and discussed in the Supporting Information (Supplementary Note 2 and Figure 35).

Improved $\text{Ni}^{2+}/\text{Ni}^{3+}$ Redox Chemistry and Enhanced Catalyst Conductivity. To understand how Co incorporation influences the kinetics of $\text{Ni}^{2+} \rightarrow \text{Ni}^{3+}$ redox charging as shown in Figure 1d, we studied the sweep-rate dependence of cyclic voltammetry. The redox current, i , exhibits classic semi-infinite diffusion in the battery-like electrode materials (generally called “bulk” charging), e.g. $i \propto \nu^{0.5}$, while the pseudocapacitive materials represent a linear current dependence on the sweeping rate (generally called “surface” charging), $i \propto \nu$.^{55,56} To deconvolute the catalytic contribution from “bulk” and “surface” active sites, we recorded the sweeping rate dependence of the redox peak on different supports. The charge, integrated from redox oxidation wave, was fit as a function of sweeping rate; thus, the fraction ratio of “surface” and “bulk” redox charging on different metal supports was attained (see Supplementary Note 3 for more details). As shown in Figure 4a, the surface reaction dominates charging process of NiFeLDH loaded on all supports at the experimental sweeping rate (see Supplementary Figures 36 and 37 for the relation-

ships between the “surface”/“bulk” charging and the sweeping rate on various supports). We next plot both the surface and bulk-stored charge with OER activity on different substrates (Figure 4b), the geometric OER current density is picked up at $\eta = 350$ mV). The current of OER has a more obvious positive correlation with the integral of surface charge than the bulk, revealing that the generation of effective active sites for OER mainly occurs on the outer surface. This provides an important insight into locating the active spots generated before OER and confirms the surface structure dominating the catalytic response of NiFeLDH. More importantly, Co support hugely improves the generation of surface active sites by $\sim 3\times$, much higher than the other metal foils. This phenomenon is attributed to the *in situ* incorporation of Co, which greatly improves the electrochemical accessibility and facilitates the generation of Ni active sites on the surface and explains the previous results of NiFeLDH being an excellent OER catalyst on Co support. We next calculated the $\text{TOF}_{\text{surface redox}}$ assuming one active site per transferred electron in the surface redox wave, and trends similar to that of $\text{TOF}_{\text{redox}}$ could be observed (Supplementary Figure 38).

In addition to improve the surface redox chemistry of $\text{Ni}^{2+} \rightarrow \text{Ni}^{3+}$, we found the produced $\text{NiFeCoO}_x\text{H}_y$ is very conductive, and can dramatically reduce the *in-plane* charge transfer resistance of NiFeLDH. We fabricated the interdigitated array microelectrodes and performed a “dual-working-electrode” experiment to *in situ* measure the electrical conductivity of catalyst under relevant OER potentials in electrolyte, inspired by the work of Boettcher *et al.*^{53,57} (see

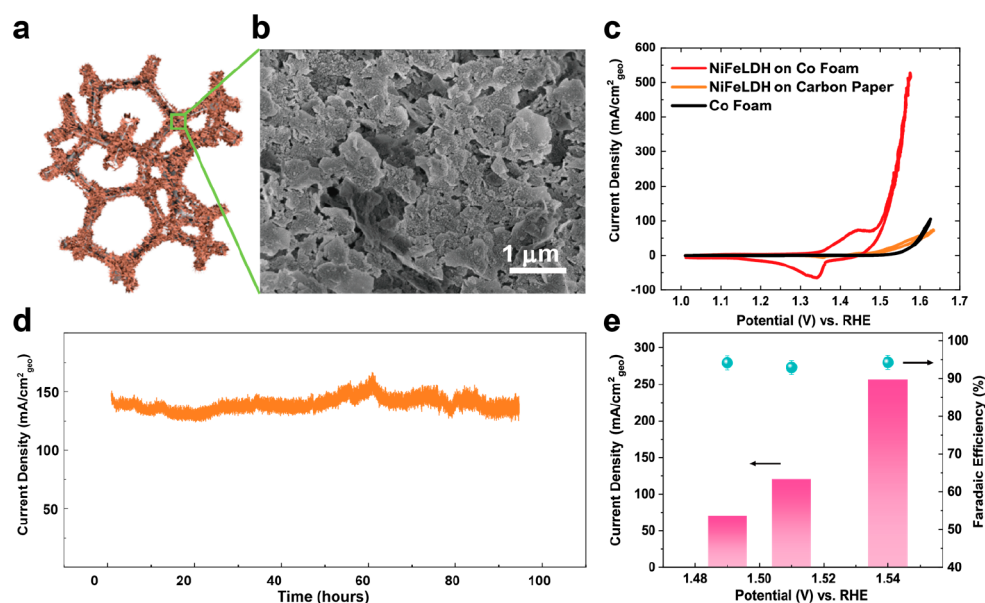


Figure 5. High-performance NiFeLDH/Co foam OER electrode for practical applications. (a and b) Schematic illustration and SEM image of NiFeLDH/Co foam. (c) OER polarization curves of Co foam with and without NiFeLDH loading and carbon paper with NiFeLDH loading (sweeping rate, 10 mV/s). (d) Durability test of NiFeLDH on Co foam at a constant potential of 1.52 V vs RHE. (e) Geometric current density and Faradaic efficiency from gas chromatography measurement of evolved O₂ at different applied potentials. All the measurements are performed in an O₂-saturated 1 M KOH electrolyte (pH 13.8).

Experimental Methods in the [Supporting Information](#) for details). The electrode consists of two Co interdigitated working electrodes, coated with NiFeLDH film ([Figure 4c](#) and [Supplementary Figure 39](#)). To compare, we also fabricated Au interdigitated electrodes. The conductivity of NiFeLDH was extracted from the steady-state current between the two working electrodes with a 10 mV offset, during which the potential of both were stepped between 1.2 and 1.8 V vs RHE. Upon increasing the applied potential, NiFeLDH shows an onset for conductivity enhancement before OER ([Figure 4d](#)). The potential dependence of the conductivity improvement demonstrates the same behavior on Co and Au electrodes; however, at each potential, the conductivity of the NiFeLDH/Co is 2 orders of magnitude higher than that of NiFeLDH/Au, dramatically reducing the charge-transfer resistance across the catalyst film.

On the basis of the above results, we confirm that the *in situ* incorporation of Co into NiFeLDH is responsible for boosting the population of activated metal centers and thus leads to an enhancement of OER activity. This *in situ* produced NiFeCoO_xH_y not only enhances by ~100× the conductivity of catalysts but also acts as active species in OER catalysis. Our study uncovers the importance of the unstable conductive supports in electrocatalysis. This synergistic effect between electrocatalyst and conductive support can also be generalized to NiFeLDH with different Fe and Ni stoichiometries, even pure Ni(OH)₂ and Fe(OH)₃ ([Supplementary Figures 40–42](#)). However, it is found that Co cannot activate the other transition-metal-based oxides without Ni and Fe, indicating that Ni/Fe is necessary for the activation, the mechanism of which is still elusive and needs further exploration.

High-Performance OER Electrode for Practical Applications. Motivated by the possibility of attaining exceptionally high activity via increasing the specific surface area of catalyst^{58–60} (total surface area per unit projected electrolyte area), we drop-cast NiFeLDH catalyst directly on a Co foam [Soochow

Taili company; purity 99.99%; porosity 95–98%; pore radius 0.3–5 mm (10–130 pores per inch)]. As shown in [Figure 5a,b](#), well-ordered hexagonal plates on porous Co support were attained, showing a low overpotential of 310 mV at 300 mA/cm² (projected geometric area) in CV ([Figure 5c](#)), which outperforms NiFeLDH directly loaded on a carbon paper as well as a large number of typical OER catalysts previously reported ([Supplementary Table 11](#)). The operating durability of the OER catalysts is also essential for their practical application. To check the performance stability of the NiFeLDH on Co foam, we ran water oxidation under a constant potential at 1.52 V vs RHE continuously over 90 h and observed no appreciable decrease of current density in this time interval ([Figure 5d](#)). By measuring the O₂ evolved from NiFeLDH/Co foam catalyst quantitatively ([Figure 5e](#)), we confirmed the high activity under three different applied potential, attaining >95% Faradaic efficiency of O₂ within our available ±1.6% experimental error (see details in [Supplementary Note 4](#)).

In this work, we demonstrate the notably distinguished OER catalytic activity of NiFeLDH on 8 flat conductive supports under equivalent conditions, concluding that the rationally designed electrocatalyst/support interface can greatly impact the overall electrocatalytic efficiency. In particular, the use of Co as a non-noble metal support greatly improves the activity of NiFeLDH by 10-fold compared to the traditional inert conductive supports such as FTO, ITO, and glassy carbon. XPS, AFM, and TEM measurements evidence that Co was incorporated into NiFeLDH during OER, leading to a porous NiFeCoO_xH_y layer. *In situ* XAS tests further demonstrate a strong synergetic effect among Ni, Fe, and Co, showing that the higher oxidative and OER catalytically active Ni (Fe) atoms with shorter Ni(Fe)–O bond length and lower coordination number were observed only in the presence of the Co support. This new discovery stresses the unique interaction among Ni, Fe, and Co and offers a new paradigm

for designing and developing highly active electrocatalytic systems via marrying catalyst and support and creating synergy. Compared with the predominant route to date to address the low activity of electrocatalyst by optimizing the composition and/or geometry of the catalytically active sites, this strategy is much easier to process and can be potentially applied in other attractive electrochemical energy conversion reactions, such as H₂ evolution, CO₂ reduction, and N₂ fixation. This work highlights the importance of a well-designed electrocatalyst/support interface and will open up a new pathway to utilize the kinetically unstable conductive support as a simple method to enhance the energy conversion efficiency.

■ ASSOCIATED CONTENT

Supporting Information

The Supporting Information is available free of charge at <https://pubs.acs.org/doi/10.1021/acseenergylett.0c01584>.

Chemicals, experimental methods, and supplementary notes and figures (PDF)

■ AUTHOR INFORMATION

Corresponding Author

Liming Zhang – Department of Chemistry, Fudan University, Shanghai 200438, China; orcid.org/0000-0001-6795-3381; Email: zhanglm@fudan.edu.cn

Authors

Haoyang Gu – Department of Chemistry, Fudan University, Shanghai 200438, China

Guoshuai Shi – Department of Chemistry, Fudan University, Shanghai 200438, China

Hsiao-Chien Chen – Department of Chemistry, National Taiwan University, Taipei 10617, Taiwan

Songhai Xie – Department of Chemistry, Fudan University, Shanghai 200438, China

Yingzhou Li – Department of Mathematics, Duke University, Durham, North Carolina 27708-0320, United States

Haonan Tong – Department of Chemistry, Fudan University, Shanghai 200438, China

Chunlei Yang – Department of Chemistry, Fudan University, Shanghai 200438, China

Chenyuan Zhu – Department of Chemistry, Fudan University, Shanghai 200438, China

J. Tyler Mefford – Department of Materials Science and Engineering, Stanford University, Stanford, California 94305-4034, United States; orcid.org/0000-0003-4965-4147

Heyi Xia – Department of Chemistry, Fudan University, Shanghai 200438, China

William C. Chueh – Department of Materials Science and Engineering, Stanford University, Stanford, California 94305-4034, United States; orcid.org/0000-0002-7066-3470

Hao Ming Chen – Department of Chemistry, National Taiwan University, Taipei 10617, Taiwan; orcid.org/0000-0002-7480-9940

Complete contact information is available at:

<https://pubs.acs.org/doi/10.1021/acseenergylett.0c01584>

Author Contributions

L.Z., H.G., and G.S. conceived the experiment. H.G., G.S., H.T., C.Y., and C.Z. fabricated the electrodes and carried out the electrochemical characterization. H.-C.C. and H.M.C. performed the in situ XAS measurements. S.X. carried out the

TEM and EDX analysis. Y.L. helped with the modeling and data fitting. All authors discussed the results and participated in writing the manuscript.

Notes

The authors declare no competing financial interest.

■ ACKNOWLEDGMENTS

This work is funded by the National Natural Science Foundation of China (Grant 21872039). L.Z. also acknowledges the financial support from National Program for Thousand Young Talents of China.

■ REFERENCES

- (1) Tauster, S. J.; Fung, S. C.; Garten, R. L. Strong metal-support interactions. Group 8 noble metals supported on TiO₂. *J. Am. Chem. Soc.* **1978**, *100*, 170–175.
- (2) Tauster, S. J. Strong metal-support interactions. *Acc. Chem. Res.* **1987**, *20*, 389–394.
- (3) Liu, X.; et al. Strong metal-support interactions between gold nanoparticles and ZnO nanorods in CO oxidation. *J. Am. Chem. Soc.* **2012**, *134*, 10251–10258.
- (4) Matsubu, J. C.; et al. Adsorbate-mediated strong metal-support interactions in oxide-supported Rh catalysts. *Nat. Chem.* **2017**, *9*, 120–127.
- (5) Bruix, A.; et al. A new type of strong metal-support interaction and the production of H₂ through the transformation of water on Pt/CeO₂(111) and Pt/CeO_x/TiO₂(110) catalysts. *J. Am. Chem. Soc.* **2012**, *134*, 8968–8974.
- (6) Tang, H.; et al. Strong metal-support interactions between gold nanoparticles and nonoxides. *J. Am. Chem. Soc.* **2016**, *138*, 56–59.
- (7) Schweitzer, N. M.; et al. High activity carbide supported catalysts for water gas shift. *J. Am. Chem. Soc.* **2011**, *133*, 2378–2381.
- (8) Lin, L.; et al. Low-temperature hydrogen production from water and methanol using Pt/alpha-MoC catalysts. *Nature* **2017**, *544*, 80–83.
- (9) Yao, S.; et al. Atomic-layered Au clusters on alpha-MoC as catalysts for the low-temperature water-gas shift reaction. *Science* **2017**, *357*, 389–393.
- (10) Dong, J.; Fu, Q.; Jiang, Z.; Mei, B.; Bao, X. Carbide-supported Au catalysts for water-gas shift reactions: a new territory for the strong metal-support interaction effect. *J. Am. Chem. Soc.* **2018**, *140*, 13808–13816.
- (11) Wang, L.; et al. Strong metal-support interactions achieved by hydroxide-to-oxide support transformation for preparation of sinter-resistant gold nanoparticle catalysts. *ACS Catal.* **2017**, *7*, 7461–7465.
- (12) Jin, H. Y.; et al. Emerging two-dimensional nanomaterials for electrocatalysis. *Chem. Rev.* **2018**, *118*, 6337–6408.
- (13) Lv, L.; Yang, Z.; Chen, K.; Wang, C.; Xiong, Y. 2D layered double hydroxides for oxygen evolution reaction: from fundamental design to application. *Adv. Energy Mater.* **2019**, *9*, 1803358.
- (14) Liu, Y.; et al. Approaching the schottky-mott limit in van der Waals metal-semiconductor junctions. *Nature* **2018**, *557*, 696–700.
- (15) Wang, Y.; et al. Van der Waals contacts between three-dimensional metals and two-dimensional semiconductors. *Nature* **2019**, *568*, 70–74.
- (16) Seh, Z. W.; et al. Combining theory and experiment in electrocatalysis: insights into materials design. *Science* **2017**, *355*, eaad4998.
- (17) McCrory, C. C. L.; et al. Benchmarking hydrogen evolving reaction and oxygen evolving reaction electrocatalysts for solar water splitting devices. *J. Am. Chem. Soc.* **2015**, *137*, 4347–4357.
- (18) Corrigan, D. A. The catalysis of the oxygen evolution reaction by iron impurities in thin film nickel oxide electrodes. *J. Electrochem. Soc.* **1987**, *134*, 377–384.
- (19) Corrigan, D. A.; Bendert, R. M. Effect of coprecipitated metal ions on the electrochemistry of nickel hydroxide thin films: cyclic voltammetry in 1M KOH. *J. Electrochem. Soc.* **1989**, *136*, 723–728.

- (20) Gong, M.; et al. An advanced Ni-Fe layered double hydroxide electrocatalyst for water oxidation. *J. Am. Chem. Soc.* **2013**, *135*, 8452–8455.
- (21) Trotochaud, L.; Young, S. L.; Ranney, J. K.; Boettcher, S. W. Nickel-iron oxyhydroxide oxygen-evolution electrocatalysts: the role of intentional and incidental iron incorporation. *J. Am. Chem. Soc.* **2014**, *136*, 6744–6753.
- (22) Friebel, D.; et al. Identification of highly active Fe sites in (Ni,Fe)OOH for electrocatalytic water splitting. *J. Am. Chem. Soc.* **2015**, *137*, 1305–1313.
- (23) Trzesniewski, B. J.; et al. In situ observation of active oxygen species in Fe-containing Ni-based oxygen evolution catalysts: the effect of pH on electrochemical activity. *J. Am. Chem. Soc.* **2015**, *137*, 15112–15121.
- (24) Chen, J. Y.; et al. Operando analysis of NiFe and Fe oxyhydroxide electrocatalysts for water oxidation: detection of Fe⁴⁺ by mossbauer spectroscopy. *J. Am. Chem. Soc.* **2015**, *137*, 15090–15093.
- (25) Gorlin, M.; et al. Oxygen evolution reaction dynamics, faradaic charge efficiency, and the active metal redox states of Ni-Fe oxide water splitting electrocatalysts. *J. Am. Chem. Soc.* **2016**, *138*, 5603–5614.
- (26) Li, N.; et al. Influence of iron doping on tetravalent nickel content in catalytic oxygen evolving films. *Proc. Natl. Acad. Sci. U. S. A.* **2017**, *114*, 1486–1491.
- (27) Stevens, M. B.; Trang, C. D. M.; Enman, L. J.; Deng, J.; Boettcher, S. W. Reactive Fe-sites in Ni/Fe (oxy)hydroxide are responsible for exceptional oxygen electrocatalysis activity. *J. Am. Chem. Soc.* **2017**, *139*, 11361–11364.
- (28) Asnavandi, M.; Yin, Y.; Li, Y.; Sun, C.; Zhao, C. Promoting oxygen evolution reactions through introducing oxygen vacancies to benchmark NiFe-OOH catalysts. *ACS Energy Lett.* **2018**, *3*, 1515–1520.
- (29) Roy, C.; et al. Impact of nanoparticle size and lattice oxygen on water oxidation on NiFeO_xH_y. *Nat. Catal.* **2018**, *1*, 820–829.
- (30) Lee, S.; Banjac, K.; Lingenfelder, M.; Hu, X. Oxygen isotope labeling experiments reveal different reaction sites for the oxygen evolution reaction on nickel and nickel iron oxides. *Angew. Chem., Int. Ed.* **2019**, *58*, 10295–10299.
- (31) Burke, M. S.; Enman, L. J.; Batchellor, A. S.; Zou, S.; Boettcher, S. W. Oxygen evolution reaction electrocatalysis on transition metal oxides and (oxy)hydroxides: activity trends and design principles. *Chem. Mater.* **2015**, *27*, 7549–7558.
- (32) Louie, M. W.; Bell, A. T. An investigation of thin-film Ni-Fe oxide catalysts for the electrochemical evolution of oxygen. *J. Am. Chem. Soc.* **2013**, *135*, 12329–12337.
- (33) Suntivich, J.; May, K. J.; Gasteiger, H. A.; Goodenough, J. B.; Shao-Horn, Y. A perovskite oxide optimized for oxygen evolution catalysis from molecular orbital principles. *Science* **2011**, *334*, 1383–1385.
- (34) Song, F.; Hu, X. Exfoliation of layered double hydroxides for enhanced oxygen evolution catalysis. *Nat. Commun.* **2014**, *5*, 4477.
- (35) Zhang, B.; et al. Homogeneously dispersed multimetal oxygen-evolving catalysts. *Science* **2016**, *352*, 333–337.
- (36) Suryawanshi, M. P.; et al. Hierarchically coupled Ni:FeOOH nanosheets on 3D N-doped graphite foam as self-supported electrocatalysts for efficient and durable water oxidation. *ACS Catal.* **2019**, *9*, 5025–5034.
- (37) Liu, J.; et al. Hierarchical NiCo₂S₄@NiFe LDH heterostructures supported on nickel foam for enhanced overall-water-splitting activity. *ACS Appl. Mater. Interfaces* **2017**, *9*, 15364–15372.
- (38) Sirisomboonchai, S.; et al. Fabrication of NiO microflake@NiFe-LDH nanosheet heterostructure electrocatalysts for oxygen evolution reaction. *ACS Sustainable Chem. Eng.* **2019**, *7*, 2327–2334.
- (39) Liu, X.; Chen, Z.; Cao, M. NiFe layered double hydroxide on nitrogen doped TiO₂ nanotube arrays toward efficient oxygen evolution. *ACS Appl. Energy Mater.* **2019**, *2*, 5960–5967.
- (40) Yeo, B. S.; Bell, A. T. Enhanced activity of gold-supported cobalt oxide for the electrochemical evolution of oxygen. *J. Am. Chem. Soc.* **2011**, *133*, 5587–5593.
- (41) Zhuang, Z.; Sheng, W.; Yan, Y. Synthesis of monodisperse Au@Co₃O₄ core-shell nanocrystals and their enhanced catalytic activity for oxygen evolution reaction. *Adv. Mater.* **2014**, *26*, 3950–3955.
- (42) Zhu, W.; et al. Au promoted nickel-iron layered double hydroxide nanoarrays: a modular catalyst enabling high-performance oxygen evolution. *ACS Appl. Mater. Interfaces* **2017**, *9*, 19807–19814.
- (43) Strickler, A. L.; Escudero-Escribano, M. A.; Jaramillo, T. F. Core-shell Au@metal-oxide nanoparticle electrocatalysts for enhanced oxygen evolution. *Nano Lett.* **2017**, *17*, 6040–6046.
- (44) Fester, J.; et al. The structure of the cobalt oxide/Au catalyst interface in electrochemical water splitting. *Angew. Chem., Int. Ed.* **2018**, *57*, 11893–11897.
- (45) Enman, L. J.; Vise, A. E.; Stevens, M. B.; Boettcher, S. W. Effects of metal electrode support on the catalytic activity of Fe(oxy)hydroxide for the oxygen evolution reaction in alkaline media. *ChemPhysChem* **2019**, *20*, 3089–3095.
- (46) Han, Y.; et al. Preparation of Ni²⁺-Fe³⁺ layered double hydroxide material with high crystallinity and well-defined hexagonal shapes. *Chem. Mater.* **2008**, *20*, 360–363.
- (47) Batchellor, A. S.; Boettcher, S. W. Pulse-electrodeposited Ni-Fe (oxy)hydroxide oxygen evolution electrocatalysts with high geometric and intrinsic activities at large mass loadings. *ACS Catal.* **2015**, *5*, 6680–6689.
- (48) Ng, J. W. D.; et al. Gold-supported cerium-doped NiO_x catalysts for water oxidation. *Nat. Energy* **2016**, *1*, 16053.
- (49) Galizzioli, D.; Trasatti, S. Work function, electronegativity, and electrochemical behaviour of metals: IV. simple electron exchange reactions. Fe²⁺/Fe³⁺ redox couple. *J. Electroanal. Chem. Interfacial Electrochem.* **1973**, *44*, 367–388.
- (50) Stoerzinger, K. A.; et al. Oxygen electrocatalysis on (001)-oriented manganese perovskite films: Mn valency and charge transfer at the nanoscale. *Energy Environ. Sci.* **2013**, *6*, 1582–1588.
- (51) Deng, J.; et al. Morphology dynamics of single-layered Ni(OH)₂/NiOOH nanosheets and subsequent Fe incorporation studied by in situ electrochemical atomic force microscopy. *Nano Lett.* **2017**, *17*, 6922–6926.
- (52) González-Flores, D.; et al. Nickel-iron catalysts for electrochemical water oxidation-redox synergism investigated by in situ X-ray spectroscopy with millisecond time resolution. *Sustain. Energy Fuels* **2018**, *2*, 1986–1994.
- (53) Burke, M. S.; Kast, M. G.; Trotochaud, L.; Smith, A. M.; Boettcher, S. W. Cobalt-iron (oxy)hydroxide oxygen evolution electrocatalysts: the role of structure and composition on activity, stability, and mechanism. *J. Am. Chem. Soc.* **2015**, *137*, 3638–3648.
- (54) Chung, D. Y.; et al. Dynamic stability of active sites in hydr(oxy)oxides for the oxygen evolution reaction. *Nat. Energy* **2020**, *5*, 222–230.
- (55) Simon, P.; Gogotsi, Y.; Dunn, B. Where do batteries end and supercapacitors begin? *Science* **2014**, *343*, 1210–1211.
- (56) Simon, P.; Gogotsi, Y. Materials for electrochemical capacitors. *Nat. Mater.* **2008**, *7*, 845–854.
- (57) Stevens, M. B.; et al. Measurement techniques for the study of thin film heterogeneous water oxidation electrocatalysts. *Chem. Mater.* **2017**, *29*, 120–140.
- (58) Lu, X.; Zhao, C. Electrodeposition of hierarchically structured three-dimensional nickel-iron electrodes for efficient oxygen evolution at high current densities. *Nat. Commun.* **2015**, *6*, 6616.
- (59) Feng, J. X.; et al. FeOOH/Co/FeOOH hybrid nanotube arrays as high-performance electrocatalysts for the oxygen evolution reaction. *Angew. Chem., Int. Ed.* **2016**, *55*, 3694–3698.
- (60) Tang, C.; Cheng, N.; Pu, Z.; Xing, W.; Sun, X. NiSe nanowire film supported on nickel foam: an efficient and stable 3D bifunctional electrode for full water splitting. *Angew. Chem., Int. Ed.* **2015**, *54*, 9351–9355.